Chinese Chemical Letters 37 (2026) 112611

Contents lists available at ScienceDirect

Chinese Chemical Letters

journal homepage: www.elsevier.com/locate/cclet

An LPS-targeted fluorescent probe for dynamic super-resolution imaging of Gram-negative bacterial outer membranes

Yi Tao[a,b], Jie Pan[a,*], Wenting Yin[a], Qinglong Qiao[a,*], Zhaochao Xu[a,b,*]

[a] State Key Laboratory of Chemical Reaction Dynamics, Dalian Institute of Chemical Physics, Chinese Academy of Sciences, Dalian 116023, China
[b] University of Chinese Academy of Sciences, Beijing 100049, China

ARTICLE INFO

Article history:
Received 2 March 2026
Revised 10 March 2026
Accepted 10 March 2026
Available online 11 March 2026

Keywords:
LPS targeting
Fluorescent probe
Rhodamine
Gram-negative bacterial outer membrane
Dynamic super-resolution imaging

ABSTRACT

The outer membrane (OM) of Gram-negative bacteria, with its unique and complex structure, serves as a critical structural foundation for their heightened pathogenicity and drug resistance. However, with a thickness of only 7–9 nm, the OM is highly fragile and undergoes continuous remodeling, making it difficult to elucidate its structural dynamics and functional mechanisms during bacterial growth, division, and host invasion. Here, we developed Rho-PMXB as an OM-specific fluorescent probe that incorporates a polymyxin-derived moiety for highly specific recognition of OM lipopolysaccharides (LPS) and a rhodamine fluorophore that confers excellent photostability and high fluorescence brightness. Rho-PMXB enables selective labeling of the OMs of various Gram-negative bacteria and supports super-resolution imaging, allowing real-time visualization of OM dynamics during bacterial growth, division, and antibiotic treatment, thereby providing insight into antimicrobial mechanisms. Furthermore, Rho-PMXB enables dynamic super-resolution imaging of pathogen-host cell interactions, visualizing OM behavior during *Porphyromonas gingivalis* invasion of human gingival epithelial (HGE) cells and revealing its interplay with the host plasma membrane and actin cytoskeleton.

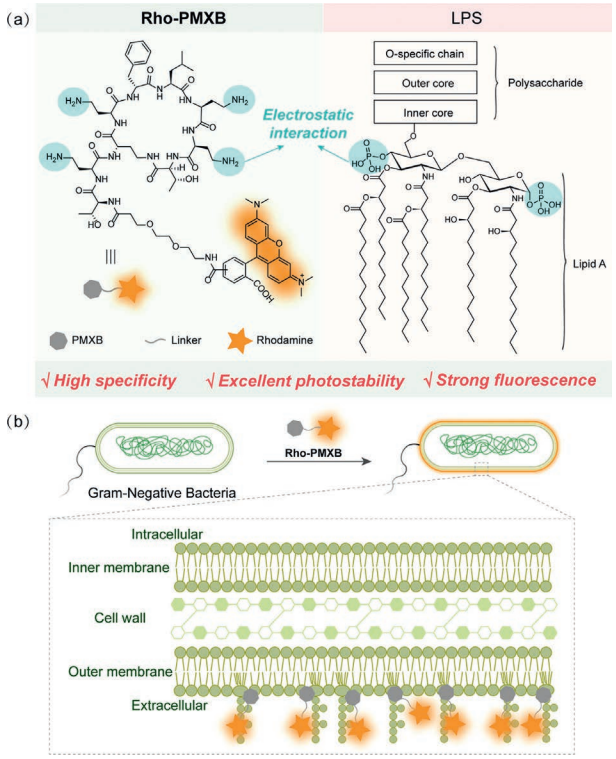
© 2026 Published by Elsevier B.V. on behalf of Chinese Chemical Society and Institute of Materia Medica, Chinese Academy of Medical Sciences.

Gram-negative bacteria pose a serious threat to global public health due to their high pathogenicity and widespread antibiotic resistance and have been designated as priority pathogens by the World Health Organization for targeted prevention and control [1,2]. Unlike Gram-positive bacteria, Gram-negative bacteria possess a unique and complex outer membrane (OM), which plays a central role in their pathogenicity and antibiotic resistance [3–5]. The OM exhibits an asymmetric bilayer architecture, consisting of an inner phospholipid leaflet and an outer leaflet primarily composed of lipopolysaccharides (LPS) and various OM proteins [6,7]. Functionally, the OM serves as a selective permeability barrier that protects bacteria from external stresses and supports survival under adverse conditions, while its LPS component can activate host immune responses and promote bacterial adhesion and invasion [8,9]. Consequently, the OM is essential for maintaining bacterial viability, mediating host infection, and enhancing antibiotic resistance [10]. Therefore, a deeper understanding of its structure and function is crucial for elucidating the pathogenic mechanisms of Gram-negative bacteria and for developing novel antibacterial strategies.

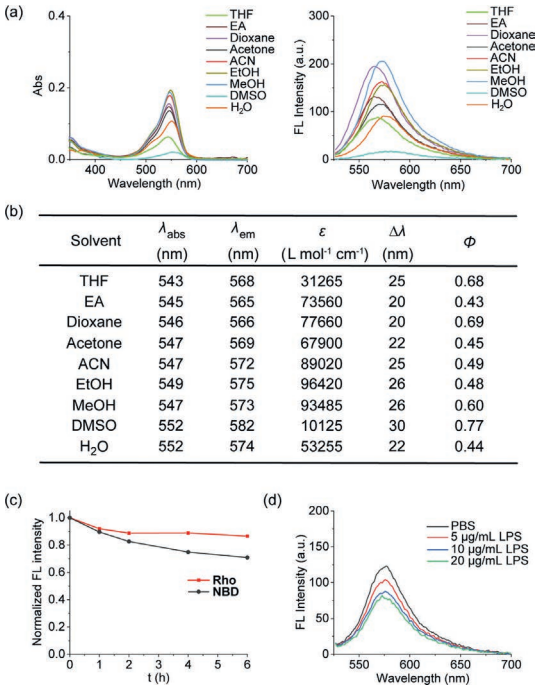
However, the OM is only 7–9 nm thick and possesses a highly refined architecture that undergoes continuous remodeling [11]. Conventional approaches such as electron microscopy provide ultrastructural information with exceptionally high spatial resolution but are limited in their ability to monitor dynamic processes in living systems [12]. As a result, direct spatiotemporal evidence of OM regulation during key biological processes such as bacterial growth, division, and host invasion remains scarce, hindering a deeper understanding of resistance development and infection control. In recent years, fluorescence imaging has emerged as an important tool for investigating the structure and dynamics of the Gram-negative bacterial OM, owing to its high sensitivity and ability to enable real-time visualization in living systems [13,14]. However, the development of OM-specific fluorescent probes remains limited, primarily because of the structural complexity and strong selective barrier properties of the OM, which make stable and selective labeling challenging. Existing membrane-targeting fluorescent probes modified with lipid chains typically rely on hydrophobic or electrostatic interactions to insert into lipid bilayers and are therefore more suitable for Gram-positive bacteria, while exhibiting poor labeling efficiency in Gram-negative bacteria due to the OM barrier [15–17]. Although FM4–64 can generate membrane-associated signals in Gram-negative bacteria, it cannot reliably distinguish between Gram-positive and Gram-negative species, resulting in in-

* Corresponding authors.
E-mail addresses: panjie@dicp.ac.cn (J. Pan), qqlqiao@dicp.ac.cn (Q. Qiao), zcxu@dicp.ac.cn (Z. Xu).

https://doi.org/10.1016/j.cclet.2026.112611
1001-8417/© 2026 Published by Elsevier B.V. on behalf of Chinese Chemical Society and Institute of Materia Medica, Chinese Academy of Medical Sciences.



Scheme 1. Design strategy and targeting mechanism of the Gram-negative bacterial OM probe Rho-PMXB. (a) Mechanism of the specific binding between Rho-PMXB and LPS. (b) Schematic illustration of the Gram-negative bacterial OM illuminated by Rho-PMXB binding to LPS.



Solvent	λ_{abs} (nm)	λ_{em} (nm)	ε (L mol^{-1} cm^{-1})	$\Delta\lambda$ (nm)	Φ
THF	543	568	31265	25	0.68
EA	545	565	73560	20	0.43
Dioxane	546	566	77660	20	0.69
Acetone	547	569	67900	22	0.45
ACN	547	572	89020	25	0.49
EtOH	549	575	96420	26	0.48
MeOH	547	573	93485	26	0.60
DMSO	552	582	10125	30	0.77
H_2O	552	574	53255	22	0.44

Fig. 1. The photophysical properties of Rho-PMXB. (a) Absorption and emission spectra of Rho-PMXB (1 μmol/L) in different solvents. λ_{ex} = 520 nm. (b) Spectroscopic data of Rho-PMXB in different solvents: peak ultraviolet-visible (UV–vis) absorption wavelength (λ_{abs}), maximum emission wavelength (λ_{em}), stokes shifts ($\Delta\lambda$), molar absorption coefficient (ε) and fluorescence quantum yield (φ). (c) Time-dependent fluorescence intensity changes at λ_{em} of Rho (1 μmol/L) and NBD (1 μmol/L) in PBS under 300 W tungsten lamp irradiation. λ_{ex} = 520 nm/490 nm. (d) Fluorescence intensity changes of Rho-PMXB after the addition of different concentrations of LPS into the test solution. $\lambda_{ex/em}$ = 520/576 nm.

sufficient specificity [18,19]. Currently reported OM-specific probes for Gram-negative bacteria commonly employ polymyxin as a targeting moiety to achieve stable binding through specific recognition of OM LPS [20–23]. However, their fluorophores are often based on dyes such as 7-nitrobenz-2-oxa-1,3-diazole (NBD) or cyanine, which generally suffer from low fluorescence brightness, limited photostability, and rapid photobleaching [24–26]. Consequently, they are mainly suitable for conventional fluorescence microscopy and fail to meet the requirements of super-resolution imaging, which demands high brightness, excellent photostability, and controllable photophysical properties [27–36]. Moreover, these probes exhibit substantial signal attenuation during long-term imaging, limiting sustained nanoscale tracking of OM structural remodeling and functional dynamics and thereby constraining real-time analysis of OM-associated biological processes. Therefore, the development of novel fluorescent probes for the Gram-negative bacterial OM that combine high brightness, excellent photostability, and strong targeting specificity, and that enable long-term super-resolution imaging of OM structure and dynamics, is of great importance for elucidating mechanisms of antibiotic resistance, pathogenicity, and host invasion, as well as for advancing OM functional studies, antibacterial drug development, and infectious disease control.

Here, we developed Rho-PMXB as a novel OM-specific fluorescent probe for Gram-negative bacteria that specifically recognizes LPS on the bacterial OM, thereby enabling selective fluorescence imaging of the OM (Scheme 1). Rho-PMXB consists of a polymyxin B-derived structure as the targeting ligand and a rhodamine fluorophore. The polymyxin-derived moiety is generated by hydrolysis of the alkyl chain of polymyxin B, which abolishes its bactericidal activity, while the amino groups retain electrostatic interactions with LPS phosphate groups, thereby preserving high OM recognition specificity and enabling stable labeling of the Gram-negative bacterial OM [37,38]. The rhodamine component provides excellent photostability and high fluorescence brightness [39,40]. As a result, Rho-PMXB combines high brightness, superior photostability, and strong specificity, enabling long-term dynamic imaging of the OM under super-resolution microscopy. Using this probe, we achieved selective labeling of various Gram-negative bacterial OMs and real-time super-resolution monitoring of OM remodeling during bacterial growth, division, and antibiotic treatment, revealing drug-induced effects on membrane structure. Furthermore, application of Rho-PMXB to *Porphyromonas gingivalis* (*P. gingivalis*) enabled visualization of OM dynamics during infection of HGE cells, providing insight into the interplay between bacterial membranes and host cells during pathogenesis.

We first synthesized Rho-PMXB by conjugating a rhodamine moiety onto a dealkylated polymyxin scaffold, and characterization by high-performance liquid chromatography (HPLC) indicated a highly pure product (Scheme S1 and Fig. S1 in Supporting information). However, due to the presence of structural isomers, the chromatogram displayed two major peaks with similar retention times and comparable intensities, attributable to configurational differences that influence elution behavior. These results confirm the successful synthesis and identity of the desired product with high purity.

To systematically evaluate the photophysical properties of Rho-PMXB, we measured its absorption and emission spectra in various solvents (Figs. 1a and b, Fig. S2 in the Supporting information). The probe consistently exhibited high fluorescence quantum yields (>0.4) across different solvents, demonstrating sufficient brightness for high-sensitivity bioimaging applications. We next assessed the photostability of Rho-PMXB in comparison with a previously reported OM probe incorporating an NBD fluorophore. Under con-

tinuous illumination with a tungsten lamp, fluorescence intensities were monitored over time. After 6 h of irradiation, the fluorescence intensity of NBD decreased to ~70 % of its initial value, whereas Rho retained over 85 % of its original intensity (Fig. 1c and Fig. S3 in Supporting information). Correspondingly, the absorption spectra of Rho exhibited only minimal changes, further confirming its superior photostability relative to NBD (Fig. S4 in Supporting information). These results indicate that Rho-PMXB maintains more stable fluorescence under prolonged excitation, making it well suited for long-term live-cell imaging. Furthermore, we performed preliminary experiments to examine the binding specificity of Rho-PMXB toward LPS (Fig. 1d). Incremental addition of LPS to the probe solution resulted in a marked decrease in fluorescence intensity. Considering the strong electrostatic and hydrophobic interactions between polymyxin and LPS, this quenching effect is attributed to local probe accumulation at LPS surfaces, which promotes rhodamine aggregation and induces aggregation-induced quenching. Although accompanied by reduced fluorescence intensity, this result supports the specific binding of Rho-PMXB to LPS, enabling selective recognition of the Gram-negative bacterial OM. In summary, Rho-PMXB exhibits high brightness, excellent photostability, and strong LPS-binding specificity, making it an effective probe for selective OM imaging and long-term dynamic tracking of Gram-negative bacteria.

Given the high fluorescence brightness, excellent photostability, and strong targeting specificity of Rho-PMXB demonstrated in vitro, we further applied this probe to fluorescence imaging of Gram-negative bacterial OMs. Five Gram-negative species (*E. coli*, *A. rhizogenes*, *C. freundii*, *S. enterica*, and *P. aeruginosa*) and four Gram-positive species (*B. cereus*, *S. epidermidis*, *E. faecalis*, and *S. aureus*) were incubated with 2 μmol/L Rho-PMXB, followed by confocal imaging (Fig. 2a and Fig. S5 in Supporting information). Strong fluorescence signals were observed along the OMs of all Gram-negative bacteria, whereas no detectable fluorescence was observed in Gram-positive bacteria. These results are consistent with the molecular design of the probe, in which the polymyxin moiety selectively interacts with LPS on Gram-negative bacterial OMs. To further evaluate the probe's discriminatory ability in mixed bacterial populations, one Gram-negative and one Gram-positive species were co-incubated with Rho-PMXB for 1 h (Fig. 2b). Confocal imaging clearly demonstrated selective labeling of only the Gram-negative bacteria, while Gram-positive cells remained non-fluorescent. This result highlights the potential of Rho-PMXB as a simple and effective molecular tool for rapid differentiation of Gram-negative and Gram-positive bacteria, supporting preliminary bacterial identification.

We next performed super-resolution imaging of the OMs of the five Gram-negative species (*E. coli*, *A. rhizogenes*, *C. freundii*, *S. enterica*, and *P. aeruginosa*) using structured illumination microscopy (SIM) and stimulated emission depletion microscopy (STED) (Figs. 2c and d). Rho-PMXB exhibited high fluorescence brightness, a favorable signal-to-noise ratio (SNR), and excellent photostability under both imaging modalities, enabling clear visualization of outer membrane structures with ~170 nm resolution and an SNR of ~2.5 under STED. In three-dimensional (3D) imaging of *E. coli*, fluorescence signals were strictly confined to the OM, with negligible cytoplasmic fluorescence, further confirming the probe's membrane-targeting specificity (Fig. S6 in Supporting information). This selective membrane localization reduces background signals arising from nonspecific internalization or probe diffusion, thereby improving imaging contrast. Overall, Rho-PMXB enables highly specific imaging of Gram-negative bacterial OMs under both confocal and super-resolution microscopy, providing high-quality membrane imaging.

Additionally, the cytotoxicity of Rho-PMXB toward Gram-negative bacteria was evaluated (Fig. S7 in Supporting information). After co-incubation with various probe concentrations for 24 h, bacterial viability remained high, indicating minimal effects on growth and proliferation and demonstrating good biocompatibility.

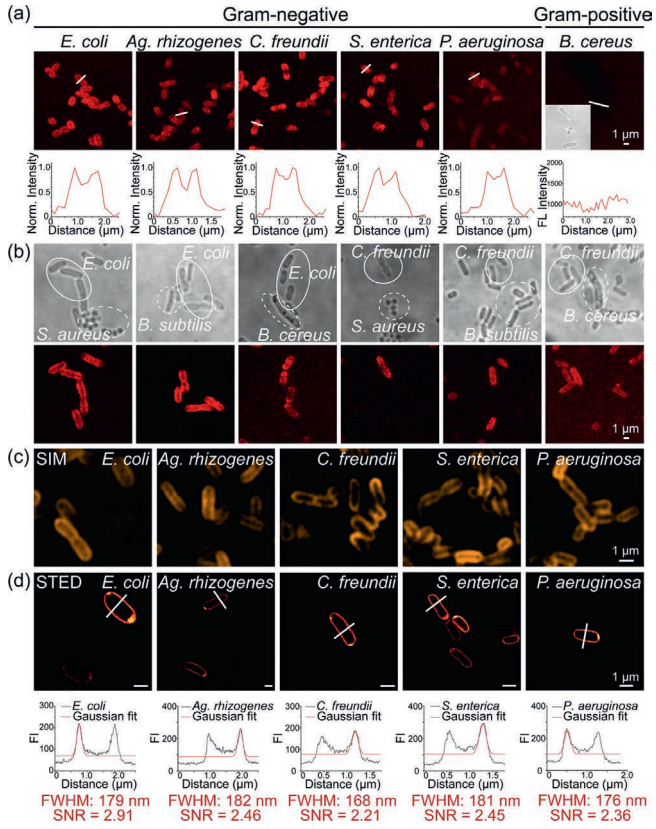


Fig. 2. Fluorescence imaging of bacterial OMs using Rho-PMXB. (a) Five kinds of Gram-negative bacteria (*E. coli*, *Ag. rhizogenes*, *C. freundii*, *S. enterica*, and *P. aeruginosa*) and one kind of Gram-positive bacteria (*B. cereus*) ($OD_{600} = 2$) were incubated with Rho-PMXB (2 μmol/L) for 1 h, followed by confocal imaging. Fluorescence intensity plots showing normalized fluorescence profiles along the lines indicated in the images. $\lambda_{ex} = 543$ nm. (b) Confocal imaging of mixed bacterial solutions containing Gram-negative bacteria (*E. coli* or *C. freundii*) and Gram-positive bacteria (*S. aureus*, *B. subtilis*, or *B. cereus*) ($OD_{600} = 2$) incubated with Rho-PMXB (1 μmol/L). $\lambda_{ex} = 543$ nm. (c) Five kinds of Gram-negative bacteria (*E. coli*, *Ag. rhizogenes*, *C. freundii*, *S. enterica*, and *P. aeruginosa*) ($OD_{600} = 2$) were incubated with Rho-PMXB (2 μmol/L) for 1 h, followed by SIM imaging. $\lambda_{ex} = 561$ nm. (d) Five kinds of fixed Gram-negative bacteria (*E. coli*, *Ag. rhizogenes*, *C. freundii*, *S. enterica*, and *P. aeruginosa*) ($OD_{600} = 2$) were incubated with Rho-PMXB (2 μmol/L) for 1 h, followed by STED imaging. Fluorescence intensity plots showing fluorescence profiles along the lines indicated in the images. $\lambda_{ex} = 561$ nm. Scale bar: 1 μm.

After confirming the excellent imaging performance of Rho-PMXB, we applied it to dynamic imaging of Gram-negative bacterial OMs. *E. coli* cells were stained and placed into a microfluidic chip to maintain viability (Figs. 3a and b), and long-term real-time SIM imaging was performed to track OM dynamics during bacterial growth, division, and antibiotic treatment. Under untreated conditions, SIM imaging revealed the dynamic behavior of *E. coli* over time (Fig. 3c). Cells exhibited gradual growth accompanied by coordinated OM expansion until entry into the division phase. Each cell ultimately divided into two daughter cells, which continued subsequent growth and proliferation. Throughout this process, SIM imaging captured progressive OM expansion, septum formation, and complete daughter-cell separation. These observations demonstrate that Rho-PMXB enables reliable tracking of nanoscale OM dynamics during dynamic biological processes. We next used Rho-PMXB to investigate the effects of different antibiotics on OM dynamics. Following ampicillin treatment, *E. coli* cells progressively enlarged but failed to divide, consistent with inhibition of cell wall

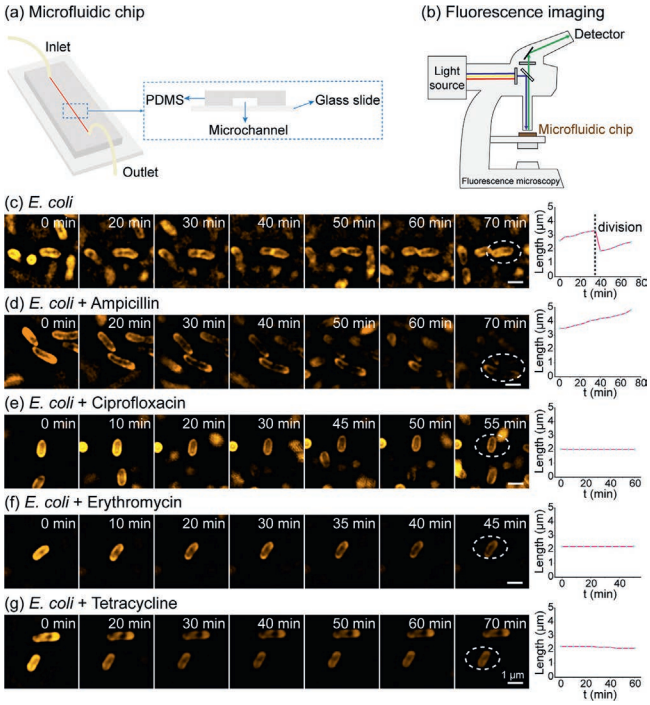


Fig. 3. Dynamic SIM imaging of the OM of *E. coli* treated with different antibiotics using Rho-PMXB in microfluidic chip. (a) Microfluidic chip schematic diagram. (b) Fluorescence imaging of bacteria in microfluidic chips. (c) Dynamic SIM imaging of *E. coli* ($OD_{600} = 1$) OM during normal growth and division after staining with 1 μmol/L Rho-PMXB for 1 h at 37 °C, with cell length monitored over time. (d-g) *E. coli* cells were treated with ampicillin (d), ciprofloxacin (e), erythromycin (f), or tetracycline (g) for 1 h, followed by staining with 1 μmol/L Rho-PMXB for 1 h at 37 °C. OM dynamics and changes in cell length over time were monitored by SIM imaging. $\lambda_{ex} = 561$ nm. Scale bar: 1 μm.

synthesis, which blocks division and ultimately leads to cell lysis (Fig. 3d). In contrast, ciprofloxacin-treated cells showed neither significant volume increase nor division, maintaining stable morphology throughout imaging, consistent with inhibition of DNA replication (Fig. 3e). Similarly, erythromycin- and tetracycline-treated cells displayed no growth- or division-related dynamics over extended imaging periods, reflecting inhibition of protein synthesis (Figs. 3f and g). Collectively, these results demonstrate that Rho-PMXB enables real-time visualization of *E. coli* growth and division while allowing dynamic monitoring of OM behavior under different antibiotic treatments. This OM phenotype-based imaging approach provides a direct, high-spatiotemporal-resolution strategy for probing antibiotic mechanisms of action. Notably, distinct OM dynamic patterns observed under different antibiotic treatments correlate closely with their known molecular mechanisms, suggesting that OM imaging may serve as a phenotypic readout for distinguishing classes of antibacterial agents. In the future, this methodology could be potentially applied to screen novel antibiotics, investigate their mechanisms of action, and support the development of precision antibacterial strategies based on membrane phenotypes.

Given that Rho-PMXB enables stable OM labeling in Gram-negative bacteria and supports long-term dynamic tracking, we sought to extend its application to more complex host-pathogen systems. In Gram-negative bacteria, pathogen invasion of host cells represents a central step in infection and disease progression [41]. This process involves multiple sequential stages, including host recognition, adhesion, invasion, and intracellular colonization and dissemination, all of which exhibit highly heterogeneous spatiotemporal dynamics [42,43]. However, due to the lack of suitable imaging tools, the dynamic behavior of the pathogen OM during invasion has remained difficult to directly visualize at

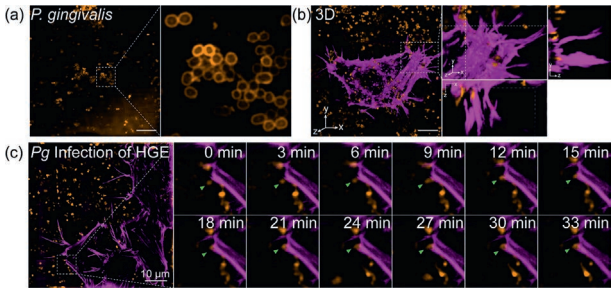


Fig. 4. SIM imaging of the interaction between *P. gingivalis* and the actin cytoskeleton in HGE cells. (a) *P. gingivalis* ($OD_{600} = 2$) were incubated with Rho-PMXB (2 μmol/L) for 1 h, followed by SIM imaging. (b) *P. gingivalis* was stained with Rho-PMXB (2 μmol/L) for 1 h, and HGE cells expressing Halo-actin were stained with SiR-Halo (100 nmol/L) for 20 min. After co-incubation of *P. gingivalis* and HGE for 6 h, 3D-SIM imaging was performed to visualize their interactions. (c) Dynamic SIM imaging of *P. gingivalis* stained with Rho-PMXB (2 μmol/L) for 1 h and Halo-actin-expressing HGE cells stained with SiR-Halo (100 nmol/L) for 20 min after 6 h of co-incubation. $\lambda_{ex} = 561$ nm/640 nm. Scale bar: 10 μm.

the nanoscale. To address this limitation, we used Rho-PMXB for specific labeling of the pathogen OM, enabling real-time super-resolution tracking of key steps in host-cell invasion and allowing dynamic visualization and mechanistic analysis of this complex biological process. We selected *P. gingivalis* and human gingival epithelial (HGE) cells as a representative pathogen-host interaction model. *P. gingivalis* is a major periodontal pathogen with well-characterized host invasion capability, and as a Gram-negative bacterium, its OM is rich in LPS, providing an ideal target for Rho-PMXB labeling. HGE cells represent the natural target of *P. gingivalis*, allowing this model to closely mimic physiological infection conditions. Although multiple virulence factors of *P. gingivalis* have been identified, the dynamic behavior of its OM during host invasion remains poorly understood due to the lack of direct visualization. Thus, this system provides an excellent platform for investigating pathogen-host interactions using Rho-PMXB.

We first validated the imaging performance of Rho-PMXB in *P. gingivalis* (Fig. 4a). SIM imaging demonstrated clear and stable labeling of the bacterial OM with high resolution. Concurrently, HGE cells transfected with Halo-actin or Halo-adrβ2 were labeled using SiR-Halo, enabling visualization of cytoskeletal structures and membrane and establishing dual-channel imaging conditions for subsequent pathogen-host interaction studies (Fig. S8 in Supporting information). During co-culture of *P. gingivalis* with HGE cells, we initially examined bacterial interactions with the actin cytoskeleton. Time-lapse imaging revealed progressive approach and tight association between *P. gingivalis* and actin structures, and 3D reconstruction showed bacteria embedded within the actin network, suggesting that adhesion or entry may be facilitated through interactions with the host cytoskeleton (Figs. 4b and c, Fig. S9 in Supporting information). However, because actin labeling does not define the cell boundary, it remained unclear whether the bacteria had actually entered the host cells.

To further determine bacterial internalization, we monitored interactions between *P. gingivalis* and membrane-labeled (Halo-adrβ2-transfected) HGE cells. Over time, *P. gingivalis* approached and interacted with the host cell membrane, with local membrane vesicle formation observed, indicating potential disruption of host membrane integrity (Fig. 5a and Fig. S10 in Supporting information). Under standard culture conditions, only close surface contacts were observed, with no definitive evidence of intracellular invasion. Considering that iron limitation enhances *P. gingivalis* invasiveness, we pre-cultured *P. gingivalis* under iron-depleted conditions for 24 h and conducted infection imaging experiments. Dynamic imaging revealed that iron-depleted *P. gingivalis* exhibited

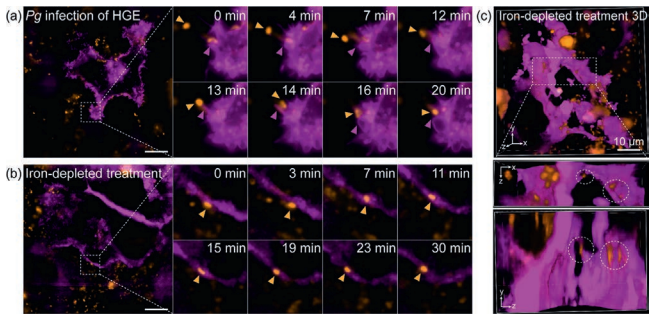


Fig. 5. SIM imaging of the interaction between *P. gingivalis* and the plasma membrane of HGE cells under different conditions. (a) Dynamic SIM imaging of *P. gingivalis* stained with Rho-PMXB (2 μmol/L) for 1 h and Halo-adrβ2-expressing HGE cells stained with SiR-Halo (100 nmol/L) for 20 min, following 6 h of co-incubation. (b) Dynamic SIM imaging of iron-depleted treatment *P. gingivalis* stained with Rho-PMXB (2 μmol/L) for 1 h and Halo-adrβ2-expressing HGE cells stained with SiR-Halo (100 nmol/L) for 20 min, following 6 h of co-incubation. (c) 3D SIM imaging of iron-depleted treatment *P. gingivalis* stained with Rho-PMXB (2 μmol/L) for 1 h and Halo-adrβ2-expressing HGE cells stained with SiR-Halo (100 nmol/L) for 20 min, following 6 h of co-incubation. λ_{ex} = 561 nm/640 nm. Scale bar: 10 μm.

enhanced adhesion and membrane embedding (Fig. 5b and Fig. S11 in Supporting information), and 3D imaging confirmed that these bacteria breached the membrane barrier and entered HGE cells, with distinct intracellular *P. gingivalis* signals providing direct visual evidence of completed invasion (Fig. 5c). This represents direct visualization of enhanced *P. gingivalis* infectivity under iron-depleted conditions. Using Rho-PMXB, we achieved super-resolution visualization of the entire process of *P. gingivalis* invading HGE cells, systematically revealing bacterial adhesion, interactions with the cytoskeleton and plasma membrane, and subsequent entry into host cells. Notably, results obtained under iron-depleted conditions provided direct evidence that iron deficiency significantly enhances the invasiveness of *P. gingivalis*. This not only broadens our understanding of the pathogenic mechanisms of *P. gingivalis* but also offers new insights into the role of the host microenvironment in pathogen invasion.

In this study, we developed a novel Gram-negative bacterial OM-specific fluorescent probe Rho-PMXB, which combines the high-affinity LPS recognition capability of polymyxin with the superior photophysical properties of rhodamine. Rho-PMXB exhibits high brightness, excellent photostability, and remarkable selectivity, enabling long-term, high-resolution imaging of bacterial OMs under live-cell conditions. Using SIM, we visualized dynamic behaviors of the *E. coli* OM during growth, division, and antibiotic treatment, providing phenotypic evidence consistent with known antibacterial mechanisms. Furthermore, we applied Rho-PMXB to investigate infection of HGE cells by the periodontal pathogen *P. gingivalis*, enabling super-resolution dynamic visualization of the entire pathogen-host interaction process. The results revealed bacterial adhesion, interactions with host cytoskeletal and plasma membrane structures, and enhanced invasion under iron-limited conditions, providing direct insights into the dynamic role of bacterial OMs during infection. Rho-PMXB offers a powerful tool for studying Gram-negative bacterial OM dynamics and pathogen-host interactions. This work advances our understanding of bacterial pathogenic mechanisms and antibacterial action modes, and provides a foundation for the development of OM-targeted antimicrobial and diagnostic strategies.

Declaration of competing interest

The authors declare that they have no known competing financial interests or personal relationships that could have appeared to influence the work reported in this paper.

CRediT authorship contribution statement

Yi Tao: Writing – original draft, Investigation, Data curation. **Jie Pan:** Writing – review & editing, Supervision. **Wenting Yin:** Formal analysis. **Qinglong Qiao:** Writing – review & editing, Writing – original draft, Supervision. **Zhaochao Xu:** Writing – review & editing, Supervision, Funding acquisition, Conceptualization.

Acknowledgments

This work is supported by the National Natural Science Foundation of China (Nos. 22225806, 22522816, 22578443, 22378385, 22278394, 22507121, 22508383, 22541705, U25A20620); The Chinese Academy of Sciences Project for Young Scientists in Basic Research (No. YSBR-104); The Energy Revolution S&T Program of Yulin Innovation Institute of Clean Energy (No. E412050705); Liaoning Binhai Laboratory (No. LBLD-2024-07); Dalian Institute of Chemical Physics (Nos. DICP I202436, DICP I202522, DICP I202512, DICP&SIA UN202502, DMU-1&DICP UN202301, DMU-1&DICP UN202302, DMU-2&DICP UN202502); Natural Science Foundation of Liaoning (Nos. 2025-MS-061, 2025-BS-0147); Dalian Science and Technology Innovation Fund Program (No. 2022JJ11CG007).

Supplementary materials

Supplementary material associated with this article can be found, in the online version, at doi:10.1016/j.cclet.2026.112611.

References

[1] Y. Ji, G. Li, J. Wang, C. Piao, X. Zhou, Molecules 27 (2022) 6440.
[2] W. Zhong, D. Zheng, X. Liao, et al., Chin. Chem. Lett. 36 (2025) 110448.
[3] W. Pajerski, D. Ochonska, M. Brzychczy-Wloch, et al., J. Nanopart. Res. 21 (2019) 186.
[4] D. Saxena, R. Maitra, R. Bormon, et al., npj Antimicrob. Resist. 1 (2023) 17.
[5] Z. Li, J. Song, X. Gao, et al., Chin. Chem. Lett. 36 (2025) 110073.
[6] E. Lundstedt, D. Kahne, N. Ruiz, Chem. Rev. 121 (2020) 5098–5123.
[7] J. Yeow, M. Luo, S.-S. Chng, Nat. Commun. 14 (2023) 8285.
[8] K.L. May, T. Akiyama, B.G. Parker, M. Kim, M. Grabowicz, mBio 16 (2025) e0251825.
[9] F. Putker, M.P. Bos, J. Tommassen, A. Filloux, FEMS Microbiol. Rev. 39 (2015) 985–1002.
[10] J. Sun, S.T. Rutherford, T.J. Silhavy, K.C. Huang, Nat. Rev. Microbiol. 20 (2021) 236–248.
[11] V.r.R.F. Matias, A. Al-Amoudi, J. Dubochet, T.J. Beveridge, J. Bacteriol. 185 (2003) 6112–6118.
[12] J.L.S. Milne, S. Subramaniam, Nat. Rev. Microbiol. 7 (2009) 666–675.
[13] S.A. Yoon, S.Y. Park, Y. Cha, L. Gopala, M.H. Lee, Front. Chem. 9 (2021) 743923.
[14] L. Dubois, A. Vettiger, J.A. Buss, T.G. Bernhardt, mBio 16 (2025) e0395024.
[15] Y. Huang, W. Chen, J. Chung, J. Yin, J. Yoon, Chem. Soc. Rev. 50 (2021) 7725–7744.
[16] W. Zhou, Q. Qiao, Y. Tao, et al., Sens. Actuat. B: Chem. 410 (2024) 135691.
[17] Y. Tao, Q. Qiao, Y. Ruan, et al., Chem. Sci. 16 (2025) 7766–7772.
[18] B. Spangler, D. Dovala, W.S. Sawyer, et al., ACS Infect. Dis. 4 (2018) 1355–1367.
[19] A. Farkas, G. Maróti, A. Kereszt, É. Kondorosi, Front. Microbiol. 8 (2017) 51.
[20] A. Baibek, Z. Konieczna, M. Üçüncü, et al., Chem. Biomed. Imaging 3 (2024) 45–50.
[21] M. Wu, S. He, H. Tang, H. Hu, Y. Shi, Front. Chem. 9 (2022) 809584.
[22] P. Bao, C. Li, H. Ou, et al., Biomater. Sci. 9 (2021) 437–442.
[23] A. Clausell, F. Rabanal, M. Garcia-Subirats, M.A. Alsina, Y. Cajal, J. Phys. Chem. B 110 (2006) 4465–4471.
[24] A.R. Akram, S.V. Chankeshwara, E.S.T. Aslam, et al., Sci. Transl. Med. 10 (2018) eaal0033.
[25] W. Wang, X. Chen, Sci. China Chem. 61 (2018) 792–796.
[26] A. Megia-Fernandez, M. Klausen, B. Mills, et al., Chemosensors 9 (2021) 117.
[27] L. Wang, M.S. Frei, A. Salim, K. Johnsson, J. Am. Chem. Soc. 141 (2018) 2770–2781.
[28] M. Minoshima, K. Kikuchi, J. Biol. Inorg. Chem. 22 (2017) 639–652.
[29] Q. Qiao, W. Liu, J. Chen, et al., Angew. Chem. Int. Ed. 61 (2022) e202202961.
[30] Q. Qiao, A. Song, K. An, et al., Angew. Chem. Int. Ed. 64 (2024) e202417469.
[31] X. Fang, Q. Qiao, Z. Li, et al., J. Am. Chem. Soc. 147 (2025) 22253–22267.
[32] J. Chen, W. Liu, X. Fang, Q. Qiao, Z. Xu, Chin. Chem. Lett. 33 (2022) 5042–5046.
[33] W. Chi, D. Tan, Q. Qiao, Z. Xu, X. Liu, Angew. Chem. Int. Ed. 62 (2023) e202306061.
[34] S. Wu, D. Hou, Q. Qiao, Z. Xu, Chem. Soc. Rev. 55 (2026) 1935–1953.
[35] X. Fang, Q. Qiao, F. Deng, Z. Xu, Chin. Chem. Lett. 36 (2025) 110980.

[36] A. Song, Q. Qiao, N. Xu, et al., Chin. Chem. Lett. 36 (2025) 110643.
[37] T. Velkov, P.E. Thompson, R.L. Nation, J. Li, J. Med. Chem. 53 (2009) 1898–1916.
[38] R.L. Danner, K.A. Joiner, M. Rubin, et al., Antimicrob. Agents Chemother. 33 (1989) 1428–1434.
[39] W. Zhou, Q. Qiao, Y. Tao, et al., Sens. Actuat. B: Chem. 376 (2023) 132980.
[40] W. Zhou, X. Fang, Q. Qiao, et al., Chin. Chem. Lett. 32 (2021) 943–946.
[41] J. Pizarro-Cerdá, P. Cossart, Cell 124 (2006) 715–727.
[42] D. Ribet, P. Cossart, Microbes Infect. 17 (2015) 173–183.
[43] J. Soni, S. Sinha, R. Pandey, Front. Microbiol. 15 (2024) 1370818.